New model for subsurface irradiance reflectance in clear and turbid waters

Pravin Jeba Dev and Palanisamy Shanmugam*

Ocean Optics and Imaging Laboratory, Department of Ocean Engineering, Indian Institute of Technology Madras, Chennai-600036, India

**pshanmugam@iitm.ac.in*

Abstract: Modeling of subsurface irradiance reflectance fields especially in turbid coastal, harbor and lagoon waters has important applications in ecology, engineering and optical remote sensing. The present study aims at exploring many possible causes of variation in the proportionality factor *f* and analyzing its effect on the subsurface irradiance reflectance in different waters. A new model is then developed to estimate this optical property as a function of the absorption coefficient (a), backscattering coefficient (b_b), incident illumination condition, and other wavelength-depth dependent factors. Implementation of this new model is examined for five types of waters with varying turbidity and chlorophyll. Model results are verified with *in situ* measurements data and compared with the results from existing models. Formulas already proposed for estimating R in the previous studies and generally expressed by $R = 0.33(b_b/(a + b_b))$ or $R = f\,(b_b/(a + b_b))$ where $f = 0.975\text{-}0.629\mu_0$ (μ_0 is the incident photons just below the sea surface) work fairly well in clear oceanic waters, but yield large errors in turbid coastal and lagoon waters due to the use of a constant value ~0.33 or the dimensionless parameter *f* which does not account for certain processes in the model (e.g., multiple scattering, depth-dependent changes in the diffuse components of solar radiation, and spectral variation in *f*). By contrast, the new model estimates the reflectances having good agreement with *in situ* data from just below the water surface and throughout the water column. The improved performance of the present model is because it includes a parameterization of the proportionality factor *f* which varies with wavelength and depends on the sun angle, inherent optical properties, and diffuse attenuation coefficients. Knowledge related to interrelationships between inherent optical properties and apparent optical properties can be used to study the variability of the subsurface reflectance in homogeneous and stratified coastal waters with respect to many possible causes of its variations.

OCIS codes: (010.4450) Oceanic optics; (010.1350) Backscattering; (290.5850) Scattering, particles.

References and links

1. K. J. Voss and A. Morel, "Bidirectional reflectance function for oceanic waters with varying chlorophyll concentrations: Measurements versus predictions," Limnol. Oceanogr. **50**(2), 698–705 (2005).
2. H. R. Gordon and A. Y. Morel, *Remote Assessment of Ocean Color for Interpretation of Satellite Visible Imagery: A Review* (Springer-Verlag, 1983), p. 114.
3. H. R. Gordon, O. B. Brown, and M. M. Jacobs, "Computed relationships between the inherent and apparent optical properties of a flat homogeneous ocean," Appl. Opt. **14**(2), 417–427 (1975).
4. A. Morel and L. Prieur, "Analysis of variations in ocean color," Limnol. Oceanogr. **22**(4), 709–722 (1977).
5. V. I. Haltrin, "About nonlinear dependence of Remote Sensing and Diffuse reflection coefficients on Gordon's Parameter," in *Current Problems in Optics of Natural Waters* (2003), p. 382.
6. A. Morel and B. Gentili, "Diffuse reflectance of oceanic waters: its dependence on Sun angle as influenced by the molecular scattering contribution," Appl. Opt. **30**(30), 4427–4438 (1991).
7. A. Morel and B. Gentili, "Diffuse reflectance of oceanic waters. II bidirectional aspects," Appl. Opt. **32**(33), 6864–6879 (1993).

#206741 - $15.00 USD Received 19 Feb 2014; revised 14 Mar 2014; accepted 15 Mar 2014; published 14 Apr 2014

8. A. Morel and B. Gentili, "Diffuse reflectance of oceanic waters. III. implication of bidirectionality for the remote-sensing problem," Appl. Opt. **35**(24), 4850–4862 (1996).
9. A. Morel, D. Antoine, and B. Gentili, "Bidirectional reflectance of oceanic waters: accounting for Raman emission and varying particle scattering phase function," Appl. Opt. **41**(30), 6289–6306 (2002).
10. J. T. O. Kirk, "Dependence of relationship between inherent and apparent optical properties of water on solar altitude," Limnol. Oceanogr. **29**(2), 350–356 (1984).
11. H. R. Gordon, "Dependence of the diffuse reflectance of natural waters on the sun angle," Limnol. Oceanogr. **34**(8), 1484–1489 (1989).
12. S. Sathyendranath and T. Platt, "Analytic model of ocean color," Appl. Opt. **36**(12), 2620–2629 (1997).
13. W. S. Pegau and J. R. V. Zaneveld, "Temperature-dependent absorption of water in the red and near-infrared portions of the spectrum," Limnol. Oceanogr. **38**(1), 188–192 (1993).
14. W. S. Pegau, D. Gray, and J. R. Zaneveld, "Absorption and attenuation of visible and near-infrared light in water: dependence on temperature and salinity," Appl. Opt. **36**(24), 6035–6046 (1997).
15. J. R. V. Zaneveld, J. C. Kitchen, and C. Moore, "Scattering error correction of reflecting-tube absorption meters," in *Ocean Optics XII* (International Society for Optics and Photonics, 1994), Vol. 26, pp. 44–55.
16. R. M. Pope and E. S. Fry, "Absorption spectrum (380–700 nm) of pure water. II. integrating cavity measurements," Appl. Opt. **36**(33), 8710–8723 (1997).
17. R. C. Smith and K. S. Baker, "Optical properties of the clearest natural waters (200–800 nm)," Appl. Opt. **20**(2), 177–184 (1981).
18. A. Albert and C. Mobley, "An analytical model for subsurface irradiance and remote sensing reflectance in deep and shallow case-2 waters," Opt. Express **11**(22), 2873–2890 (2003).
19. T. Hirata and N. K. Højerslev, "Relationship between the irradiance reflectance and inherent optical properties of seawater," J. Geophys. Res. **113**(C3), C03030 (2008).
20. C. S. Roesler and E. Boss, "Spectral beam attenuation coefficient retrieved from ocean color inversion," Geophys. Res. Lett. **30**(9), 1468 (2003).
21. A. Bricaud, M. Babin, A. Morel, and H. Claustre, "Variability in the chlorophyll-specific absorption coefficients of natural phytoplankton: Analysis and parameterization," J. Geophys. Res. **100**(C7), 13321–13332 (1995).
22. S. P. Tiwari and P. Shanmugam, "An evaluation of models for the satellite-estimation of phytoplankton absorption coefficients in coastal / oceanic waters," IEEE J. Sel. Top. Appl. Earth Obs. Remote Sens. **7**(1), 364–371 (2014).
23. D. McKee, M. Chami, I. Brown, V. S. Calzado, D. Doxaran, and A. Cunningham, "Role of measurement uncertainties in observed variability in the spectral backscattering ratio: a case study in mineral-rich coastal waters," Appl. Opt. **48**(24), 4663–4675 (2009).
24. V. I. Haltrin, "One-parameter two-term Henyey-Greenstein phase function for light scattering in seawater," Appl. Opt. **41**(6), 1022–1028 (2002).
25. D. Stramski, A. Bricaud, and A. Morel, "Modeling the inherent optical properties of the ocean based on the detailed composition of the planktonic community," Appl. Opt. **40**(18), 2929–2945 (2001).
26. D. Sun, Y. Li, Q. Wang, H. Lv, C. Le, C. Huang, and S. Gong, "Partitioning particulate scattering and absorption into contributions of phytoplankton and non-algal particles in winter in Lake Taihu (China)," Hydrobiologia **644**(1), 337–349 (2010).
27. C. E. Binding, D. G. Bowers, and E. G. Mitchelson-Jacob, "Estimating suspended sediment concentrations from ocean color measurements in moderately turbid waters; the impact of variable particle scattering properties," Remote Sens. Environ. **94**(3), 373–383 (2005).
28. D. G. Bowers, C. E. Binding, and K. M. Ellis, "Satellite remote sensing of the geographical distribution of suspended particle size in an energetic shelf sea," Estuar. Coast. Shelf Sci. **73**(3-4), 457–466 (2007).

1. Introduction

Subsurface irradiance reflectance (also referred to as diffuse reflectance, R) plays an important role in determining rates of photosynthesis by phytoplankton and microphytes (thus setting limits on the productivity of marine ecosystems), determines the apparent color of the water body which is important for ocean color remote sensing, and influences the range and inherent visual contrast of the submerged object which varies inversely with the irradiance reflectance (thus having great significance for diving and engineering operations and for visual interactions). The quantitative study of irradiance reflectance is therefore extremely important for the above applications. The irradiance reflectance of a water body is defined as an important apparent optical property (AOP) that depends not only on the inherent optical properties (IOPs) of the seawater but also on the parameters of illumination. It is a dimensionless quantity which can be calculated just beneath the sea surface. The irradiance reflectance differs from the remote sensing reflectance R_{rs} by the bidirectional structure [1]. R is used in the theory of ocean color remote sensing to study the nature of the constituents of the seawater [2]. R is not the property of the water by itself but also a property of the diffuse light fields which vary with the depth and solar angle.

#206741 - $15.00 USD Received 19 Feb 2014; revised 14 Mar 2014; accepted 15 Mar 2014; published 14 Apr 2014

Several researchers have developed models for estimating R based on the IOPs in the last few decades. Earlier studies on R [3,4] showed that the irradiance reflectance can be related to IOPs by a constant $f = 0.33$ with the Gordon's parameter b_b/a or $b_b/(a + b_b)$ [5]. The later parameter is generally consistent with the spectral shape of the irradiance reflectance. However, the f factor plays a very important role in the determination of R [6–9]. Though the proportionality factor f is wavelength-dependent, for simplicity it is often considered as a constant in many studies. Morel and Gentili [7] expressed f as a function of the ratio of the molecular backscattering to total backscattering η_b ($= b_{bw}(\lambda)/b_b(\lambda)$), single scattering albedo ϖ and solar zenith angle $\cos(\theta_{sun})$. Kirk improved the accuracy of f as a function of the incident light flux on the sea surface (based on sun's angle) [10]. In this work, he explained the phenomena throughout the vertical column that the incident photons become deflected obliquely from its original direction due to the scattering effect. However, the model provides fairly good results just below the sea surface (especially in clear oceanic waters) but does not quantify or measure the dependable parameters that occur throughout the water column. Gordon predicted the variation of R as a function of the solar zenith angle and its dependency on the shape of the volume scattering function through Monte Carlo simulation [11]. Though this simulation study assessed the role of f on the reflectance at just below the sea surface, the complex variation of reflectance along the depth with the complex illumination and water column conditions was ignored for brevity. Sathyendranath and Platt [12] developed an analytic model of ocean color in which the variation of f was discussed for two different cases (molecular and particle scattering) based on the upwelling and downwelling average cosines. Since the main focus of the previous studies was on the interpretation of ocean color data, existing models are applicable only for homogeneous and upper ocean waters. Besides, the previously established f for Case 1 waters (based on the numerical simulation results) is not appropriate for Case 2 waters where its variation is influenced by many factors (other than the sun angle). Since the factor f for varying concentrations of the seawater constituents and its variation throughout the water column is not discussed in any of the previous studies, it becomes necessary to estimate f as a function of the other dependable parameters in various types of waters as well as throughout the water column.

The objectives of this research work are to study the variation in f and develop a model for predicting this parameter in a wide range of waters. The influence of upwelling and downwelling diffuse attenuation coefficients and solar zenith angle on the f parameter is studied in detail. Finally, a new model is developed to estimate subsurface reflectance and its variations in five different water types encountered within coastal and lagoon regions. The performance of the new model is assessed by comparing its results with *in situ* data and those from existing models.

2. Data and methods

2.1 In situ data

Six cruises were conducted to collect the various IOP and AOP profile data in turbid coastal waters off Point Calimere (Palk Strait), relatively clear waters off Chennai and eutrophic (lagoon) waters on the southeast coast of India during 14-22 May 2012, 24 February - 2 March 2013, 8 October 2013, 8 November 2013, 10 November 2013 and 16 December 2013. The characteristics of these waters generally differ from other regional waters with high levels of chlorophyll, suspended sediments, and dissolved organic matter. Such optically-complex water conditions affect the standard bio-optical algorithms to produce large errors in the derived geophysical products. For better clarity, we classify these data into five types (waters) based on the relative increase or decrease of the chlorophyll and suspended sediment levels [Fig. 1, Table 1]. Among these data sets, Type I and II data were collected from relatively clear waters off Chennai, Type III and IV data from turbid coastal waters off Point Calimere, and Type V data from eutrophic waters (lagoon waters). The range of *Chl* concentrations for Type I clear waters varied from 0.24 to 0.36 mg m^{-3} and *SS* concentrations from 0.70 to 0.83 g m^{-3}. For Type II relatively clear waters, *Chl* and *SS* range from 1.88 to 4.39 mg m^{-3} and

#206741 - $15.00 USD Received 19 Feb 2014; revised 14 Mar 2014; accepted 15 Mar 2014; published 14 Apr 2014

2.03-6.14 g m^{-3} respectively. In Type III waters, *Chl* varies from 13.22 to 18.2 mg m^{-3} and *SS* from 3.54 to 7.86 g m^{-3}. Concentrations of *Chl* and *SS* in Type IV waters range from 1.02 to 1.24 mg m^{-3} and 13.33-21.59 g m^{-3} respectively. The Type V waters are eutrophic in nature with high *Chl* (20.76-59.73 mg m^{-3}) and *SS* (3.54-27.57 g m^{-3}) concentrations.

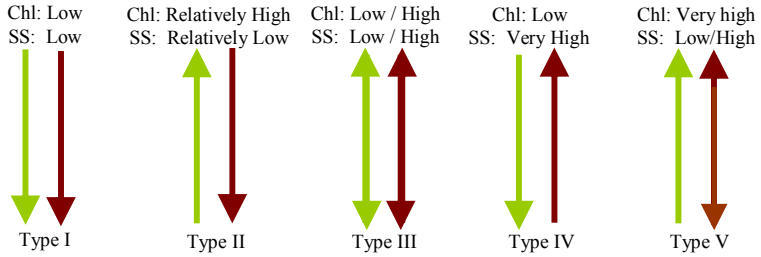

Fig. 1. Systematic diagram showing the different types (water types) of *in situ* data used in this study [also see Table 1]. Green arrows indicate *Chl* and brown arrows indicate *SS*. The arrows pointing upwards and downwards represent high and low levels of these constituents.

Table 1. Classification of water types for this study

Classification	Nature of waters	*Chl*	*SS*	Water Types
Case 1 waters	Clear waters	Low	Low	Type I
	Relatively clear	Relatively High	Relatively Low	Type II
	Relatively turbid	High/Low	Low/High	Type III
	Turbid (*SS*) waters	Low	Very High	Type IV
Case 2 waters	Eutrophic waters	Very high	Low/high	Type V

2.2 IOP measurements

The vertical profiles of IOPs and other properties were measured with WETLabs AC-S, BB9 and FLNTU sensors. The AC-S instrument was calibrated with Milli-Q ultrapure water and used to measure the absorption coefficient *'a'* and beam attenuation coefficient *'c'* across the entire visible-NIR wavelengths (350-750nm). These measurements were subjected to corrections for the temperature, salinity and scattering effects. Because the pure water absorption is dependent on the water temperature [13] and the seawater absorption is dependent on the salinity [14], absorption data were corrected using the measured water temperature and the reference temperature. Since the temperature and salinity affect the absorption coefficient and attenuation coefficient equally, similar corrections were applied to the measured beam attenuation coefficients as well. After the correction of temperature and salinity effects on the measured absorption data, scattering correction was applied to these data [15]. Finally, the particulate absorption (a_t-a_w) and attenuation spectra (c_t-c_w) were obtained after eliminating pure water absorption and attenuation coefficients (a_w and c_w) from the total absorption and total attenuation coefficients (a_t and c_t). In order to calculate the total absorption and beam attenuation coefficients, the pure water absorption and scattering coefficients taken from Pope and Fry [16] and Smith and Baker [17] were used. The particulate backscattering coefficients in the visible-NIR region were determined from VSF measurements made with a WETLabs BB9 sensor (412, 440, 488, 510, 532, 595, 650, 676 and 715nm). Vertical profiles (depth) of the absorption, attenuation and backscattering coefficients were obtained to study the inhomogeneous effects of the water column properties on the reflectance. In addition, chlorophyll fluorescence and turbidity were measured by a FLNTU sensor. Physical properties of the seawater such as conductivity, temperature and depth were measured by a SBE-CTD sensor to support the data processing and analysis.

#206741 - $15.00 USD Received 19 Feb 2014; revised 14 Mar 2014; accepted 15 Mar 2014; published 14 Apr 2014

2.3 AOP measurements

The vertical profiles of AOPs were obtained with RAMSES Trios radiometers in the visible-NIR region (350-900nm; this includes the UV range as well). These measurements included the upwelling radiance, upwelling irradiance, and downwelling irradiance. The irradiance reflectance was subsequently calculated for each station using $R = E_u/E_d$. Careful measurements were made to avoid overshadowing of the ship during the deployments at discrete depths. The diffuse attenuation coefficients K_u and K_d for different depth layers were calculated from upwelling and downwelling irradiances using the following relationship,

$$K_{u,d}(\lambda, z_1 \leftrightarrow z_2) = \left(\frac{1}{z_2 - z_1}\right)\left[\ln\left(\frac{E_{u,d}(z_1)}{E_{u,d}(z_2)}\right)\right]. \quad (1)$$

where z_1 and z_2 are the two different depth intervals for which the diffuse attenuation coefficients were calculated. These data sets were used to assess the validity of the reflectance model in clear and turbid coastal waters.

3. Theoretical background

Upwelling and downwelling light streams of solar radiant flux at a given depth are often measured by scientists to study the optical properties of natural waters. Thus, the irradiance reflectance or irradiance ratio just below the sea surface is defined as,

$$R(0^-, \lambda) = \frac{E_u(0^-, \lambda)}{E_d(0^-, \lambda)}. \quad (2)$$

where E_u is the upwelling irradiance ($mWcm^{-2}\mu m^{-1}$) and E_u is the downwelling irradiance ($mWcm^{-2}\mu m^{-1}$) just below the sea surface. R is interesting because it is relatively easy to measure *in situ*, and it is generally used in the theory of ocean color remote sensing since variations in R at the near-surface depth determine intrinsic color of the ocean. R can be related to the inherent optical properties (IOPs), such as backscattering coefficient $b_b(m^{-1})$ and absorption coefficient $a(m^{-1})$. Note that the IOPs are all wavelength dependent and their notation λ is omitted throughout this paper for brevity. Generally, R can be expressed by the following relationship,

$$R(0^-, \lambda) = f\left(\frac{b_b}{a + b_b}\right). \quad (3)$$

(For Case 1 waters $b_b << a$, thus Eq. (3) reduces to $R = fb_b/a$ according to Morel and Prieur [4]). Coefficients of absorption *'a'* and backscattering *'b_b'* are expressed as the sum of contributions from the sea water constituents,

$$a(\lambda) = a_w(\lambda) + a_p(\lambda) + a_{CDOM}(\lambda). \quad (4)$$

$$b_b(\lambda) = b_{bw}(\lambda) + b_{bp}(\lambda). \quad (5)$$

where a_w, a_p, and a_{CDOM} are the absorption coefficients due to pure water, particulate matter and colored dissolved organic matter respectively. b_{bw} and b_{bp} are the backscattering coefficients due to pure water and particulate matter respectively. According to Morel and Prieur [4], f is a varying dimensionless factor equal to 0.33. If b_b is not smaller than a, it is better to use the factor f that relates R to the ratio $b_b/(a + b_b)$. Previous studies and numerical simulations [3] yielded this relation with good accuracy in case of open ocean waters *($b_b/a \leq 0.33$)* of homogeneous and infinite depth.

#206741 - $15.00 USD Received 19 Feb 2014; revised 14 Mar 2014; accepted 15 Mar 2014; published 14 Apr 2014

$$R(0^-,\lambda) = 0.33\left(\frac{b_b}{a+b_b}\right). \tag{6}$$

Later, Kirk [10] showed the relationship between the apparent and inherent optical properties affected by available photons.

$$f = 0.975 - 0.629\cos\mu_0 . \tag{7}$$

$$R(0^-,\lambda) = (0.975 - 0.629\cos\mu_0)\left(\frac{b_b}{a+b_b}\right). \tag{8}$$

For clear waters, the factor f is linearly related to incident photons (μ_0) just below the sea surface. Several models that rely on all three components of the seawater have been developed using Hydrolight simulation results [12,18,19], in which the factor f is found to depend on the IOPs and external conditions [9]. Albert and Mobley [18] parameterized f as a function of the inherent optical properties, solar zenith angle, viewing angle and the wind speed based on the Hydrolight simulations. Gordon [11] has shown through Monte Carlo simulation that the variation of the irradiance reflectance of natural waters at null depth with sun angle is dependent on the shape of the volume scattering function (VSF) of the medium, which is important in governing the spatial structure of the radiative field.

4. A new model

The irradiance reflectance for open ocean water at depth $z = 0$ is generally parameterized [e.g., Eq. (6)] based on Monte Carlo simulation and other procedures and this relationship is found to hold satisfactory for zenith sun in a number of situations. Further, most of the previous studies aimed at analyzing the reasons for variation in ocean color so that it can be used in the theory ocean color remote sensing [3,12]. Such simple approximations are valid for infinitely deep waters, where only the water body with low chlorophyll and associated constituents contribute to the reflected signal and a parameterization of the proportionality factor f can be a constant or simply related to sun geometry and the IOPs. In Case 2 waters, the error of using a constant factor f is increased significantly. To date, other possible causes of variation in f including its spectral- and depth-dependent changes in turbid coastal waters have not been studied or explored. Consequently, an improper parameterization based on the Case 1 f affects the estimated R in Case 2 waters.

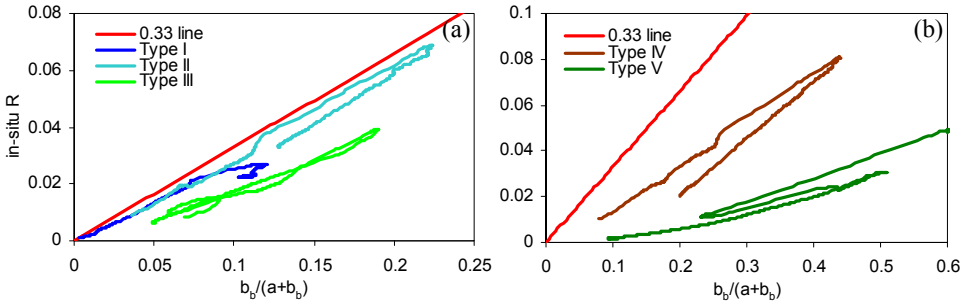

Fig. 2. *In situ R* versus $b_b/(a + b_b)$ showing the variations in slope *'f'* for different types of waters.

The factor f is the slope between R and the Gordon's parameter, $b_b/(a + b_b)$. Thus, plotting R against the Gordon's parameter for various types of waters could result in variable slopes which would deviate considerably from the reference (Case 1) slope value 0.33 with respect to many possible causes of variation in f. Figures 2(a) and 2(b) depict the variations of f in five different water types, where the red lines indicate the reference $f = 0.33$, the lines with other colors (blue, cyan and green) represent the Type I, II and III waters [Fig. 2(a)], and the lines

#206741 - $15.00 USD Received 19 Feb 2014; revised 14 Mar 2014; accepted 15 Mar 2014; published 14 Apr 2014

with brown and dark green colors represent the Type IV and V waters [Fig. 2(b)]. Note that the *f* values lie well below the reference (red) line indicating its variations in different waters. Clearly, these plots demonstrate that the simplest procedure for trying to model *R* as a function of *f = 0.33* (still valid for relatively clear waters – see the blue and cyan lines being reasonably closer to the red lines) is not adequate for turbid and eutrophic waters. As stated above, the irradiance reflectance just below the sea surface is dependent on the *f* function, IOPs and illumination condition. To extend the analysis to more complex situations (turbid and eutrophic waters), *f* should be modeled for just below the sea surface and throughout the water column. Thus, modeling of the *f* values in the present study mainly focuses on its magnitude variation, spectral variation and depth variation.

4.1 The function 'f' just below the sea surface

The function *f* just below the sea surface is modeled by taking into account its magnitude and spectral variations. The model equation of *f* is given below,

$$f(0^-,\lambda) = f(400)\left\{1 + (k_{Chl}(\lambda)\times[Chl]^2) + (k_{ss}(\lambda)\times SS)\right\}. \qquad (9)$$

The term *f(400)* determines the magnitude and the rest of the term determines the spectral variation in $f(0^-,\lambda)$ [Fig. 3]. *f(400)* is the slope parameter between *R* and the Gordon's parameter for the wavelength 400nm which is largely dependent on the light field established [10] within the region of just below the sea surface. The factors k_{Chl} and k_{SS} are the spectral constants for *Chl* and *SS* respectively (considering a wide range of their variations) [Table 2]. For the calculation of $f(0^-,\lambda)$, the wavelength 400nm is chosen as an appropriate wavelength for the reason that its dependent parameters at this wavelength are more easily quantifiable than at other wavelengths. Though it can be also achieved from other wavelength regions, the dependencies of solar angles and absorption coefficients are much more complex at these wavelengths. Thus, the spectral constants k_{Chl} and k_{SS} are modeled with respect to the wavelength of 400nm. The *Chl* used here was measured by a FLNTU sensor and the concentration of suspended sediments (*SS*) was derived from *SS* = (2.46 × *Turbidity*) + 0.3 using the *in situ* data from relatively clear and turbid waters.

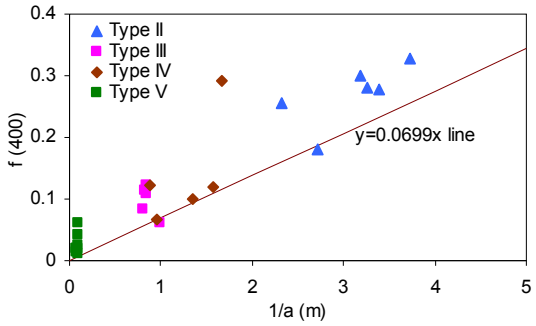

Fig. 3. The relationship between *f*(400) and (1/*a*). It explains the magnitude of the *f* component which strongly depends on the inverse of absorption coefficient *(1/a)* [plotted for 400nm]. The straight line *y = 0.0699x* is the minimal value for *f* when the sun is at nadir position.

The magnitude or slope of *f* at 400nm just below the sea surface has a strong relation to the inverse of absorption coefficient, *'1/a'*. Coastal and lagoon waters determined by the relatively high absorption coefficients (i.e., Type II, III, IV and V) have markedly low *f* values while the relatively clear waters with low absorption coefficients (Type I) have a very weak effect on the magnitude of *f*. Figure 3 reveals that the *f* values for Type V waters (high chlorophyll case) are less than 0.08 (shown in green) and ~0.1-0.15 for Type III and IV waters (pink and brown points). For Type II waters, *f* falls around 0.33 or little lesser (blue points) where the dependency of *f* on solar zenith angle is more evident. For minimum solar zenith angles and given absorption coefficients (400nm), *f(400)* lies approximately on the straight

#206741 - $15.00 USD Received 19 Feb 2014; revised 14 Mar 2014; accepted 15 Mar 2014; published 14 Apr 2014

line *(y = 0.0699x)* as shown in Fig. 3. For increasing solar zenith angles and certain specific absorption coefficients, *f* would increase significantly. This phenomenon is clearly seen in Type V and IV waters, with almost the same absorption coefficients but with varying solar zenith angles (see the green and pink points extending vertically upward in Fig. 3), indicating the influence of solar zenith angles on the *f* parameter. The straight line is the optimized fit of *f(400)* for the zenith sun (θ_s = 0°). The scattered points above this line represent the dependency of *f*(*400*) on θ_s which is defined by the optimized power function. For clear waters (Type I) with weak absorption coefficients, *f* can be approximated to be dependent of the solar zenith angle; i.e., $f = (0.0043 \times \theta_s) + 0.2$ when *Chl*<1 mg m^{-3}. However, other waters with *Chl*>1 mg m^{-3}, *f* varies in magnitude and spectral shape. Thus, *f(400)* can be calculated as follows,

$$f(400) = 0.0699 \times \left(\frac{1}{a(400)} \right) \left[1 + 0.039 (\theta_s)^{0.3} \right]. \tag{10}$$

where *a* is the total absorption coefficient at 400nm and θ_s is the solar zenith angle.

Table 2. Spectral coefficients of k_{Chl} and k_{SS} at three nanometer intervals.

λ	$k_{Chl} \times 100$	k_{SS}	λ	$k_{chl} \times 100$	k_{SS}	λ	$k_{chl} \times 100$	k_{SS}
400	0	0	508	0.0181	0.0441	616	0.0360	0.0398
404	0	0.0022	512	0.0219	0.0452	620	0.0335	0.0398
408	0.0001	0.0050	516	0.0269	0.0460	624	0.0297	0.0398
412	0.0001	0.0067	520	0.0324	0.0463	628	0.0271	0.0402
416	0.0001	0.0085	524	0.0367	0.0469	632	0.0264	0.0403
420	0.0001	0.0106	528	0.0408	0.0472	636	0.0274	0.0396
424	0.0001	0.0130	532	0.0446	0.0473	640	0.0293	0.0394
428	0.0001	0.0161	536	0.0482	0.0476	644	0.0314	0.0402
432	0.0001	0.0188	540	0.0508	0.0479	648	0.0335	0.0399
436	0.0002	0.0205	544	0.0536	0.0483	652	0.0336	0.0392
440	0.0002	0.0227	548	0.0562	0.0490	656	0.0315	0.0373
444	0.0003	0.0252	552	0.0581	0.0498	660	0.0279	0.0355
448	0.0004	0.0279	556	0.0602	0.0499	664	0.0242	0.0323
452	0.0005	0.0295	560	0.0617	0.0505	668	0.0208	0.0301
456	0.0007	0.0317	564	0.0621	0.0510	672	0.0191	0.0291
460	0.0009	0.0333	568	0.0612	0.0515	676	0.0204	0.0274
464	0.0011	0.0341	572	0.0594	0.0517	680	0.0225	0.0286
468	0.0014	0.0354	576	0.0573	0.0518	684	0.0279	0.0298
472	0.0018	0.0366	580	0.0549	0.0516	688	0.0394	0.0299
476	0.0035	0.0378	584	0.0522	0.0519	692	0.0553	0.0287
480	0.0037	0.0390	588	0.0501	0.0520	696	0.0722	0.0266
484	0.0038	0.0402	592	0.0486	0.0519	700	0.0886	0.0237
488	0.0052	0.0413	596	0.0468	0.0510	704	0.1016	0.0199
492	0.0064	0.0416	600	0.0438	0.0518	708	0.1090	0.0155
496	0.0079	0.0422	604	0.0421	0.0493	712	0.1100	0.0131
500	0.0102	0.0428	608	0.0411	0.0444	716	0.1104	0.0116
504	0.0141	0.0436	612	0.0386	0.0413			

#206741 - $15.00 USD Received 19 Feb 2014; revised 14 Mar 2014; accepted 15 Mar 2014; published 14 Apr 2014

4.2 The function 'f' throughout the water column

When dealing with any parameter throughout the water column, inhomogeneous conditions need to be taken into consideration. Unfortunately, numerical simulations of the underwater light fields based on the radiative transfer models are often biased by these conditions (in addition to the surface and bottom boundary conditions, which are complex to consider but rather simplified in those models [11]), and hence limit a detailed analysis of the factors causing the variation in f throughout the water column. Since many coastal regions are generally inhomogeneous, depth-wise measurements are highly necessary in order to study changes in the water column properties in a more realistic manner. Because of the diffuse nature of the downwelling and upwelling irradiance fields beneath the surface of a flat water surface (lagoon case) as well as situations with more complex illumination (coastal and ocean cases) under the non-uniform water column (IOPs) and bottom conditions (slope and composition), Eq. (6) cannot be applied directly to calculate R in such waters. Thus, f is derived as a function of the varying diffuse light fields with respect to the depth and expressed along with the available f (Eq. (10) just below the surface [$f(0^-,\lambda)$] as follows,

$$f(\lambda,z) = f(0^-,\lambda)\times e^{-K_u z}\times e^{+K_d z}. \tag{11}$$

$$= f(0^-,\lambda)\times e^{-K_u z + K_d z}.$$

$$f(\lambda,z) = f(0^-,\lambda)\times e^{-(K_u - K_d) z}. \tag{12}$$

The (+) sign in the exponential K_d term indicates the positive direction of light (downwelling) toward the depth and the (-) sign in the exponential K_u term indicates the direction of light traveling opposite to the downwelling light. In other terms, the f function is influenced by the respective increase and decrease of the vertical diffuse attenuation coefficients of the upwelling and downwelling light fields (both are not equal in optically complex waters). Both the diffuse attenuation coefficients K_u and K_d influence the f through a balancing act as discussed in a later section (Discussion section).

The reflectance at different depths can now be expressed as,

$$R(\lambda,z) = f(\lambda,z)\left(\frac{b_b}{a+b_b}\right). \tag{13}$$

Substituting Eqs. (9) and (10) in Eq. (12), we get

$$R(\lambda,z) = f(400)\left[1+[k_{Chl}(\lambda)\times(Chl)^2]+[k_{ss}(\lambda)\times SS]\right]\times\left(\frac{b_b}{a+b_b}\right)e^{-(K_u-K_d)z}. \tag{14}$$

The new parameterization gives more accurate results than any other models since it produces R at any discrete depths in turbid coastal and lagoon waters, which are determined by the highly varying IOPs and diffuse light field conditions.

5. Results

5.1 Description of IOP data

The inherent optical properties of the classified waters are quite interesting as they have distinct patterns in their spectral shapes [Fig. 4]. The particulate attenuation coefficient $(c_t\text{-}c_w)$ follows a decreasing trend with wavelengths for all the five water types. Significant variations are seen in the slope and magnitude (because of particle size [20],) of these spectra. In particular, Type I waters have low attenuation values 0.38-0.53 m^{-1} at 400nm, Type II waters have large variation in their $(c_t\text{-}c_w)$ spectra but with similar slopes, Type III waters have $(c_t\text{-}c_w)$ values ranging from 3 to 4 m^{-1} at 400nm (with gentle slope), and Type IV and V have relatively steep slopes with very high $(c_t\text{-}c_w)$ values (8-16 m^{-1} and 15-50 m^{-1} respectively) due

#206741 - $15.00 USD Received 19 Feb 2014; revised 14 Mar 2014; accepted 15 Mar 2014; published 14 Apr 2014

to high SS and chlorophyll (phytoplankton) concentrations [Figs. 4(a)–4(e)]. The particulate absorption coefficients (a_t-a_w) generally have two peaks in their spectra, one at 443nm and the other at 670nm [21,22].

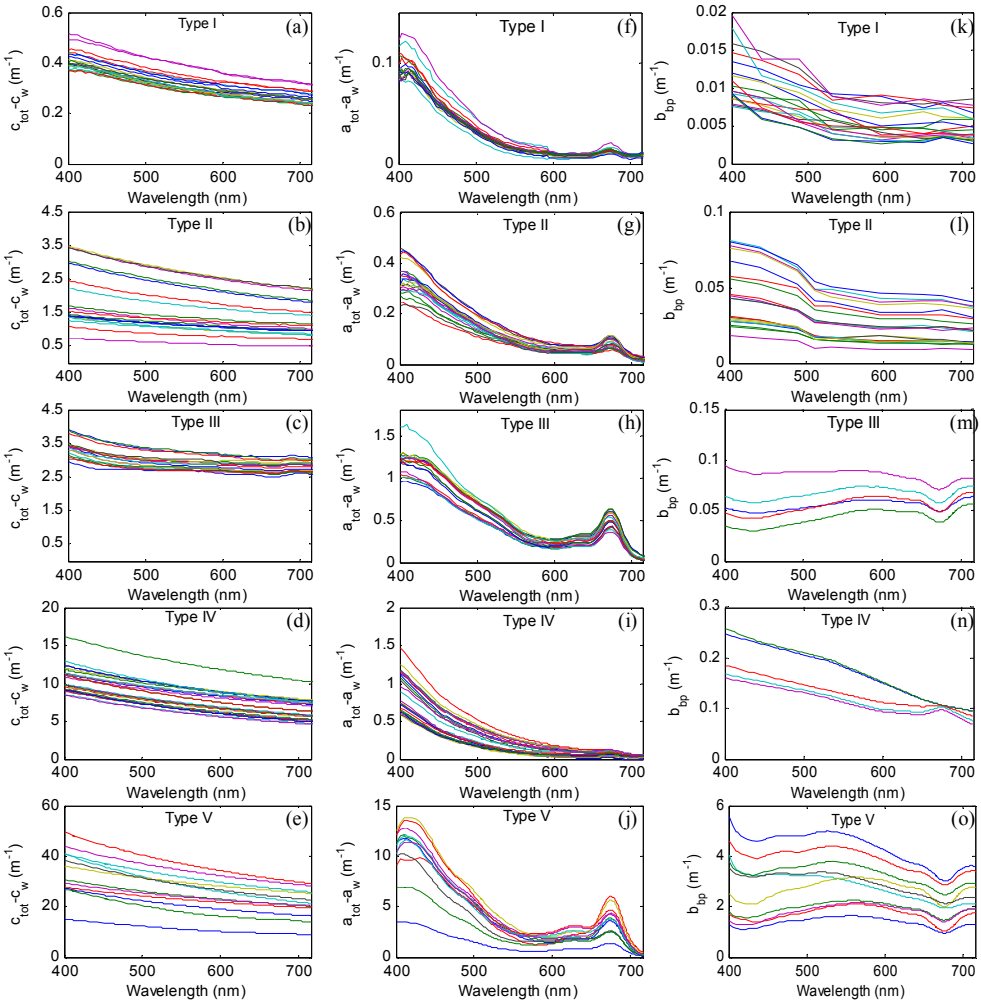

Fig. 4. Spectral plots of the *in situ* IOPs such as the particulate beam attenuation, particulate absorption and particulate backscattering coefficients used in this study.

These two peaks are clearly noticeable in Type I, II, III and V waters due to the presence of chlorophyll [Figs. 4(f), 4(g), 4(h), 4(j)]. With the increasing chlorophyll concentrations these absorption peaks are more distinct in Type III and V waters. Because of low chlorophyll contents, Type IV waters do not exhibit any such peaks at 443nm because of high levels of suspended sediments [Fig. 4(i)]. Interestingly, the particulate backscattering spectra (b_{bp}) differ from each other [Figs. 4(k)–4(o)]. For Type I, II and IV waters the b_{bp} values are generally low in the NIR and increase with decreasing wavelengths. In highly turbid and lagoon waters where optical backscattering is strongly influenced by inorganic and organic particles and where a high level of turbidities (often > 20NTU) is found in a small geographic area, the BB9 sensor tends to saturate at different backscattering levels for each channel [23] (though AC-S could still measure both absorption and attenuation coefficients allowing to derive scattering coefficients at many visible wavelengths). To obtain more reliable backscattering data, we converted the measured scattering coefficients to backscattering coefficients using a method proposed by Haltrin [24], especially for Type III and Type IV

#206741 - $15.00 USD Received 19 Feb 2014; revised 14 Mar 2014; accepted 15 Mar 2014; published 14 Apr 2014

waters dominated by exceedingly high levels of turbidity (caused by algal blooms and associated detrital/ sediment particles). Figures 4(m) and 4(o) show the spectral features of particulate backscattering for these two cases, where the broad backscattering features (maximum) are found in the green and NIR regions due to chlorophyll and a minimum combined effect of pigment and water absorption. These spectral features of the phytoplankton-dominated waters are consistent with the modeling and field studies [25,26].

5.2 Comparison of the new model with other models

To assess the relative performance of the present model, its results are compared with *in situ* data from the five water types and those of the previous models of Morel and Prieur [4], Morel and Gentili [7], Kirk [10], Albert and Mobley [18], and Hirata and Højerslev [19] [Figs. 5 and 6]. The *in situ* reflectance spectra show that for clear waters (Type I), *R* peaks toward the blue region due to high backscattering and diminishes toward the NIR region due to profound absorption by water itself. In relatively clear (Type II) and sediment-laden (turbid) waters (Type IV), the reflectance peak shifts toward the green region with significantly higher values in the red and NIR regions. The magnitude of *R* in the red and NIR regions increases with increasing sediment concentrations. On the contrary, algal bloom waters (Type III) have unique absorption and reflectance characteristics, with a minimal *R* in the blue region due to the combined absorption by phytoplankton pigments, colored dissolved organic matter (CDOM) and non-algal/detrital particles (NAP), a maximal *R* (primary peak) in the green region due to the minimal values of total absorption, a minimal *R* in the red region (around 670nm) due to the chlorophyll absorption, a high *R* (secondary peak) around 685-700nm due to the chlorophyll fluorescence, and a lower *R* in the NIR region (>700 nm) due to the increased absorption by seawater itself. In lagoon waters dominated by dense green algal blooms (Type V), the *R* spectra are distinct because of the maximum absorption of phytoplankton in the red region and maximum reflection (due to the combined effect of high backscattering and fluorescence) in the NIR region (>700 nm). These maximum absorption and reflection features tend to cause a shift in the red-edge position to longer wavelengths when increasingly high pigment content occurs. Clearly, the present model predicted *R* closely matching with the *in situ R* spectra for all the five water types, whereas the reflectance spectra produced by other models have large discrepancies with the measured *R* spectra. Among these models, the Morel and Prieur [4], Morel and Gentili [7] and Kirk [10] models appear to produce relatively better results for Type I waters but yield large errors (overestimation) for other waters (Type II-Type V). The Albert and Mobley [18] model produces very low *R* values in Type I-Type IV waters though its results being closer to the *in situ R* spectrum for lagoon waters (Type V). On the contrary, the Hirata and Højerslev [19] model estimates *R* much higher than the *in situ R* spectra and those of the other four models for Type I-Type IV waters [Fig. 6]. It also fails to produce good results for lagoon waters (Type V). These results suggest that since the *f* values are relatively lower for Case 2 waters than for Case I waters, the existing models tend to produce abnormal *R* values in both turbid coastal and lagoon waters. By contrast, the new model enables more accurate estimates of *R* for all these waters.

5.3 Irradiance reflectance just below the sea surface

To further assess the model performance, its results are compared with *in situ* data from two different discrete depths (for brevity) for four different stations in five water types [Fig. 7]. Note that for lagoon waters the comparisons are made at just below the water surface due the absence of data from different depths. It becomes apparent that the reflectance spectral curves for these waters are clearly distinguishable and more distinct from one another. The variations in the reflectance spectra between these waters are primarily due to the presence of varying levels of chlorophyll, suspended sediments and dissolved substances. The Type I waters (first two rows – just below the surface and at depth *z*) exhibit high *R* values at λ <510nm and very low *R* values at λ > 600nm. The model effectively reproduces such variations as captured in the *in situ R* data from all four stations. In Type II and IV waters, the increased absorption in

#206741 - $15.00 USD Received 19 Feb 2014; revised 14 Mar 2014; accepted 15 Mar 2014; published 14 Apr 2014

the blue region causes the reflectance peak to shift towards the right (~560-570nm) and the increased backscattering due to the presence of *Chl* and *SS* concentrations gives rise to higher reflectances in the longer wavelengths (>600nm).

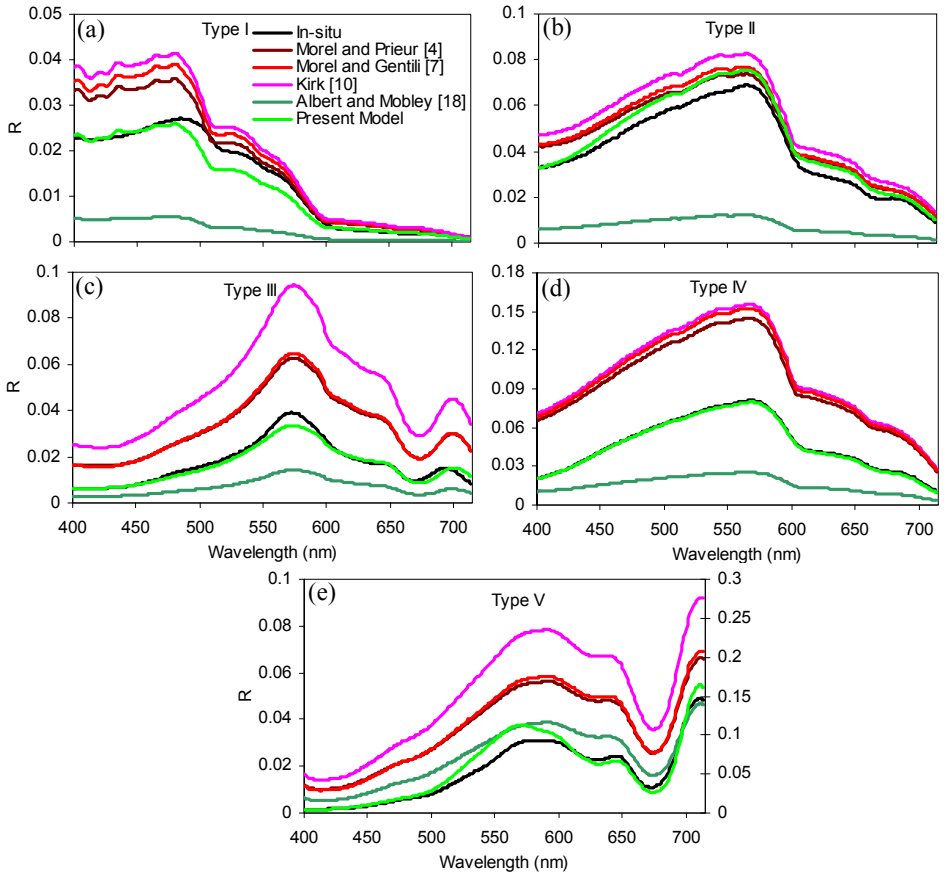

Fig. 5. Comparison of the model reflectance *(R)* with the *in situ R* spectra in five types of waters. Note that for Type V waters, the brown, red and pink lines (Morel and Prieur [4], Morel and Gentili [7] and Kirk [10] models) follow the *R* values in the secondary Y-axis.

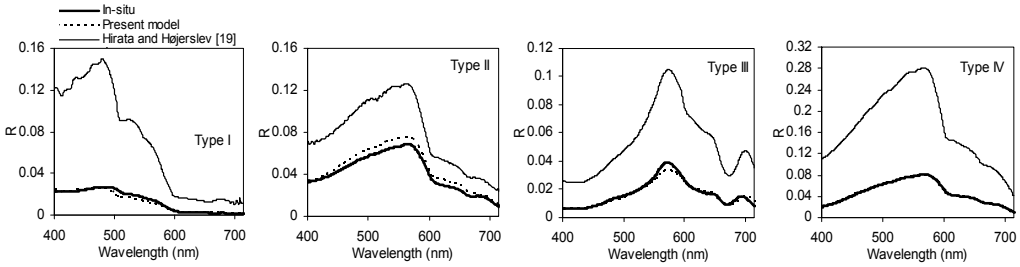

Fig. 6. Comparison of the present model with *in situ R* and the Hirata and Højerslev [19] model for the four types of waters. Due to the absence of *in situ* data for different depths in lagoon waters, the model results are not shown for Type V waters.

#206741 - $15.00 USD Received 19 Feb 2014; revised 14 Mar 2014; accepted 15 Mar 2014; published 14 Apr 2014

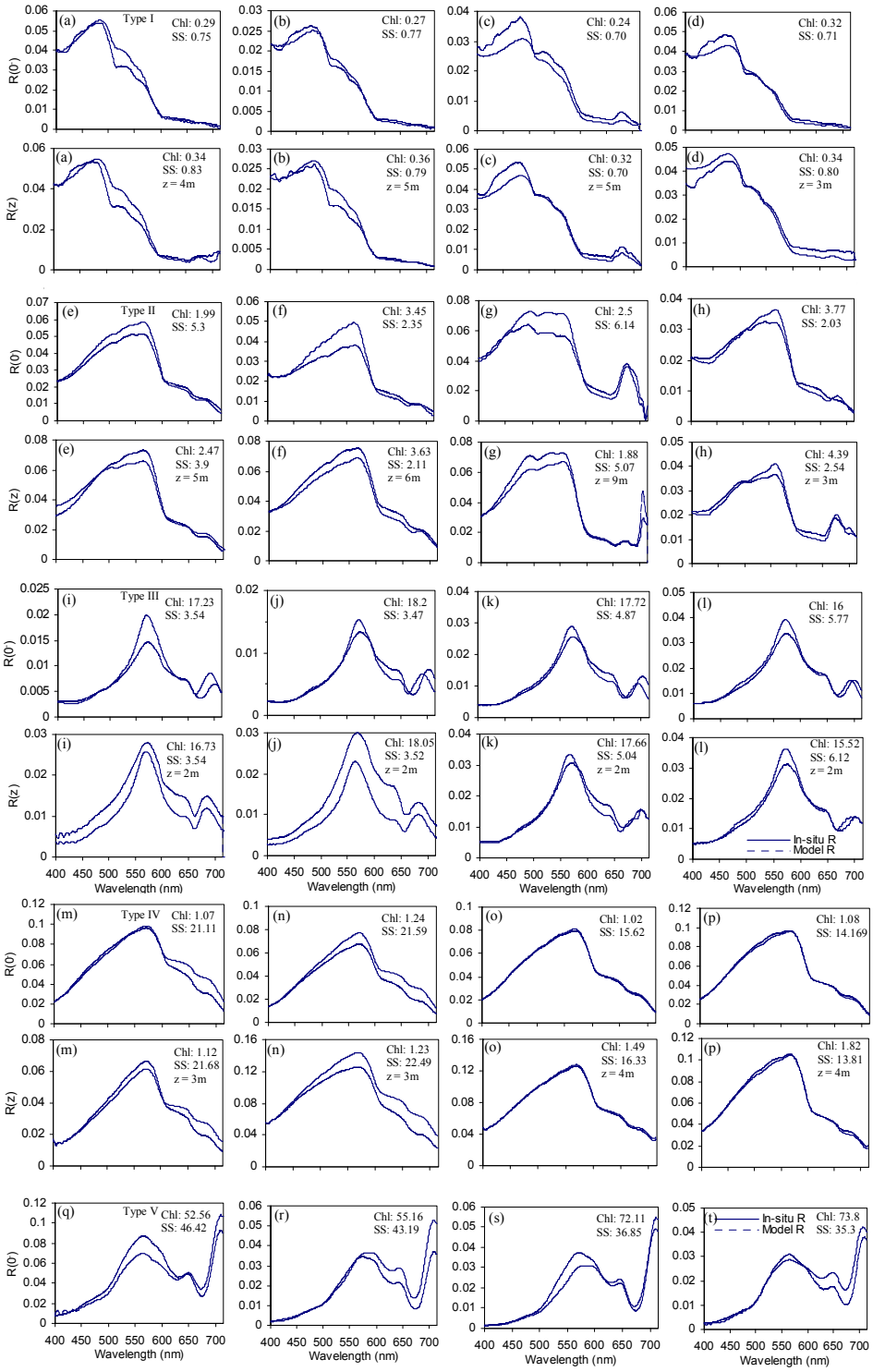

Fig. 7. Spectral comparison of the model and *in situ* reflectances at just below the water surface '*R(0-)*' and at depths '*R(z)*' for four different stations in five different water types with varying levels of *Chl* and *SS* concentrations.

#206741 - $15.00 USD Received 19 Feb 2014; revised 14 Mar 2014; accepted 15 Mar 2014; published 14 Apr 2014

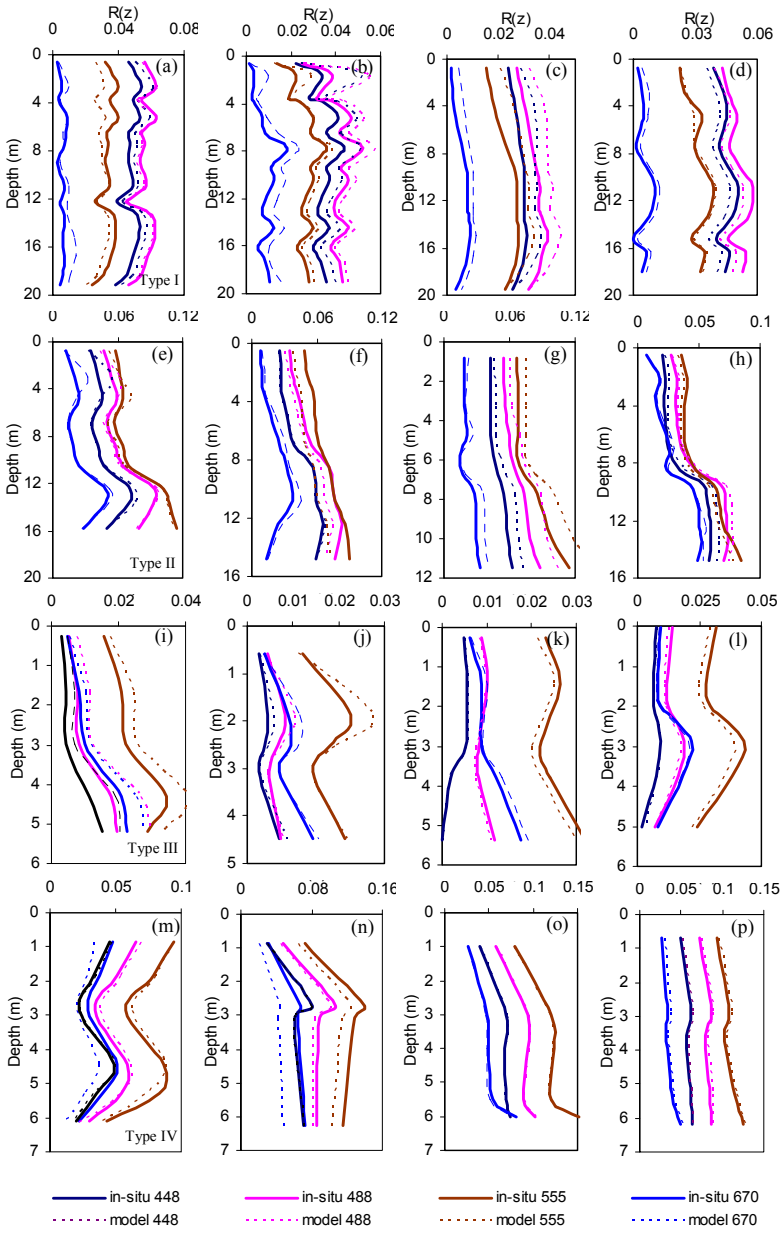

Fig. 8. Comparison of the vertical profiles of the model and *in situ R* in Type I-IV waters (top to bottom, row-wise) at four different stations (column-wise).

The Type III waters are phytoplankton-dominated waters (with $15.2<Chl<18.2$ mg m^{-3} and $3.47<SS<6.12$ g m^{-3}) showing a narrow peak (with reduced peak width) around 560-570nm, a trough in the blue and red regions and a secondary peak around 680-687nm. In some cases, the presence of inorganic sediments may suppress these red peaks as observed in Type II and IV waters [25,26]. However, in Type III waters, the concentration of suspended sediments is proportionally much lesser than the *Chl* concentration causing the secondary peak to become more pronounced around 685nm. On the contrary, the Type V waters (eutrophic waters with $52.5<Chl<73.8$ mg m^{-3} and $35.3<SS<46.42$ g m^{-3}) are highly dominated by dense algal blooms and suspended sediments showing interesting reflectance

#206741 - $15.00 USD Received 19 Feb 2014; revised 14 Mar 2014; accepted 15 Mar 2014; published 14 Apr 2014

patterns uncommon to all other waters types. These elevated chlorophyll and suspended sediment concentrations (due to low tidal incursions) cause the primary peaks to become more broadened (like sediment-dominated waters – Types II and IV types) and the secondary peaks to get further shifted to longer wavelengths (like land vegetation). For all these water types, the present model has proved its ability to better reproduce the measured reflectance spectra.

5.4 Comparison of the depth profiles of the model and in situ reflectance data

Figures 8(a)–8(p) show the comparisons of the depth profiles of the model and *in situ* reflectance values for four different stations (column-wise) from Type I-IV waters (row-wise) [corresponding to Fig. 7]. These vertical profiles clearly demonstrate that the model *R* profiles throughout the depth are nearly similar with the *in situ R* profiles, and the increase and decrease in the reflectances are primarily due to the Gordon's parameter *'$b_b(a + b_b)$'*. It means that the high backscattering / low absorption values generally produce high reflectances and the high absorption / low backscattering values yield low reflectances. Though this is true, in addition to the Gordon's parameter, *f* also plays a key role in the determination of *R*. Since *f* is dependent on the upwelling and downwelling light fields [Eq. (12)], its influence is much stronger than the Gordon's parameter in the water column (depth-wise). Thus, the Gordon's parameter plays a very important role in the spectral determination of *R*, whereas the parameter *f* plays an important role in the determination of *R* along the depth (water column).

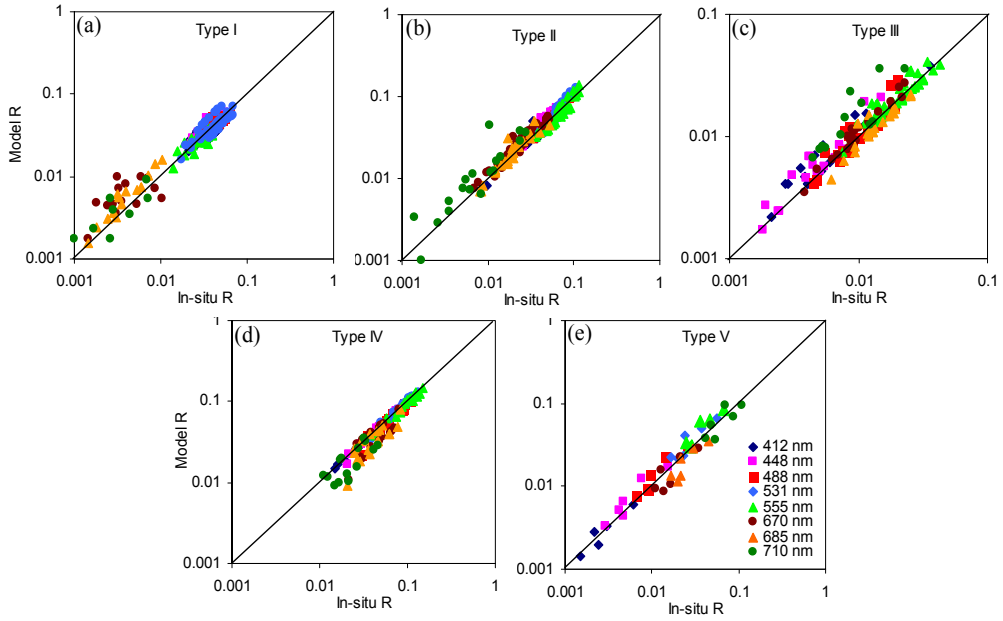

Fig. 9. Scatterplots of the model and *in situ R* for five different types of waters (at eight key wavelengths 412, 448, 488, 531, 555, 670, 685, 710nm).

5.5 Scatter plots

Figures 9(a)–9(e) show the scatterplots of the model and *in situ R* values at some key wavelengths (412, 448, 488, 531, 555, 670, 685 and 710nm) for the five types of waters (Types I-V). The model and *in situ R* values for Type I waters appear closer as they are aligned on the 1:1 line [Fig. 9(a)]. It provides good estimates of *R* at the blue and green wavelengths although having little errors as evident from the slightly scattered data at NIR (710nm). Similar performance is also observed in relatively clear Type II waters [Fig. 9(b)] for which the model *R* values at higher wavelengths are much closer to the *in situ R* values (except a few data at 710nm). For Type III waters, the model data are well dispersed around

#206741 - $15.00 USD Received 19 Feb 2014; revised 14 Mar 2014; accepted 15 Mar 2014; published 14 Apr 2014

the 1:1 line for all the selected wavelengths indicating good agreement with the *in situ R* [Fig. 9(c)]. In Type IV and V waters (sediment-dominated and bloom waters), the model and *in situ R* values are tightly consistent [Figs. 9(d)–9(e)]. Statistical analyses further confirm the closeness of these data with very low MRE (mean relative error), RMSE (root means square error), bias, and intercept, and high slope and R^2 values [Table 3]. These results apparently suggest that the overall performance of the model is good and remains valid for all the water types considered in this study.

Table 3. Statistical comparison of the model and *in situ R* for the selected wavelengths

	RMSE	*MRE*	*Bias*	*Slope*	*Intercept*	R^2	*N*
412	0.0425	–0.00001	–0.0001	0.957	0.0018	0.993	134
448	0.1119	0.0221	0.0395	1.0132	0.0016	0.9541	134
488	0.1896	0.0225	0.0361	0.9863	0.0014	0.8251	134
531	0.3029	0.0271	0.0391	0.9628	0.0018	0.5134	134
555	0.3297	0.0283	0.035	0.9653	0.0009	0.4538	134
670	0.2697	–0.016	–0.031	0.8352	0.0038	0.7128	134
685	0.2951	–0.0406	–0.078	0.7868	0.0031	0.7046	134
710	0.4253	0.0139	0.0261	0.8548	0.0038	0.6899	134

6. Discussion

The present model has been rigorously tested using *in situ* data and its results have been compared with those of the existing models in five different types of waters. These results indicated that the new model performs much better than the other models in terms of reproducing the shape and magnitude of *R* in these waters. The key issue addressed in this study is related to the *f* factor and its variation which have not been thoroughly investigated in the previous studies. At just below the sea surface, *f* is more dependent on the incident photons. However, the direction of these incident photons is obliquely deflected toward the seabed (depth) from its original path giving rise to the increment/decrement in the vertical diffuse attenuation coefficients (even for homogeneous IOP conditions), which causes *f* to vary with depth more rapidly than that at just below the surface. For high scattering waters, photons travel more oblique resulting in the increase of upwelling photons to an extent that initiates the change within the attenuation coefficients. The term *'$(K_u$-$K_d)$'* in the exponential part of Eq. (12) explains this change well and its effect on *R(λ, z)*. Toward the depth, both K_u and K_d seem to play a dominant role.

The depth-wise increase/decrease of *f* is purely dependent on the K_u and K_d [Eq. (12)]. The term $e^{-(K_u - K_d)z}$ in the *f(λ, z)* part accounts for the variation of the depth-wise reflectances. To address the depth-wise reflectance variations in the water column, three typical (inhomogeneous) examples of *R*(448) from three different stations are shown in Figs. 10(a)–10(c). Figure 10(a) shows a decreasing reflectance trend throughout the depth. At a depth of 3m, the upwelling diffuse attenuation coefficient increases more than the downwelling diffuse attenuation coefficient i.e. *(K_u>K_d)* [see Table 4]. Since K_u>K_d, the exponential term becomes negative (i.e., $e^{-(K_u - K_d)z}$) and thereby causes decreased *f(λ, z)* [Eq. (12)]. The decrease in *f(λ, z)* causes *R* to decrease at this depth. A similar trend is noticed at other depths (3.58, 4.56 and 5.72m) as well, causing *R* to further decrease with the increasing depth. Alternatively, a case of increasing reflectance is shown in Fig. 10(b). Here, K_u is lower than the K_d [Table 5] causing the exponential term to become positive. The positive term boosts the Gordon's parameter to go higher, thereby resulting in high reflectances. The increase in reflectance values is also observed throughout the water column as the K_d continues to dominate K_u. The final case is a mixture of the first two cases [Fig. 10(c)]. The reflectance continues to decrease till 3m; it increases at 4.3m and again decreases beyond 5m [Table 6]. The K_u dominates K_d at depths of 1.83 and 2.87m causing a decreased reflectance trend; at a depth of 4.4m K_d becomes dominant and increases the *R*. At depths of 5.2 and 6.1m, the domination of K_u over

#206741 - $15.00 USD Received 19 Feb 2014; revised 14 Mar 2014; accepted 15 Mar 2014; published 14 Apr 2014

K_d results in the decreased R once again. The above phenomenon conveys that when the upwelling diffuse attenuation coefficient (K_u) is very high, the upwelling light is more attenuated and seizes the light escaping from its layer (particular depth). As a result, low reflectance is observed. Conversely, when $K_d > K_u$, the weaker K_u allows the upwelling light to escape and hence the increase in the reflectance is observed.

The f values for relatively clear and turbid waters (this study) are relatively lower than those already reported in the literature (for low chlorophyll Case I waters). As the f values are determined by the IOPs and light fields in the water column, K_u and K_d are the most appropriate terms to be considered in the model because they are determined by both the IOPs and diffuse light fields. From the above analyses we infer that K_u and K_d may be a responsible factor for the fluctuation of f values in bloom and turbid waters. For many oceanic waters, it was found that $K_u \approx 2K_d$ [27,28]. However, our field measurements from relatively clear and turbid waters confirm that K_u is approximately equal to K_d, i.e. $K_u \approx K_d$ [see Tables 4, 5, 6]. Since K_u is relatively lower than K_d, it gives a way for the light to escape in the upward direction to a greater extent. In addition, it is important to note that f varies with latitudes as well [27]. For the Irish Sea, for the overhead sun f ranges from 0.4 to 0.5 [28]. As the new model is based on the above evidences from a wide range of waters, it provides accurate estimates of R and its variations in different types of waters encountered within the study region (e.g., estuaries/lagoons, coastal and clear waters).

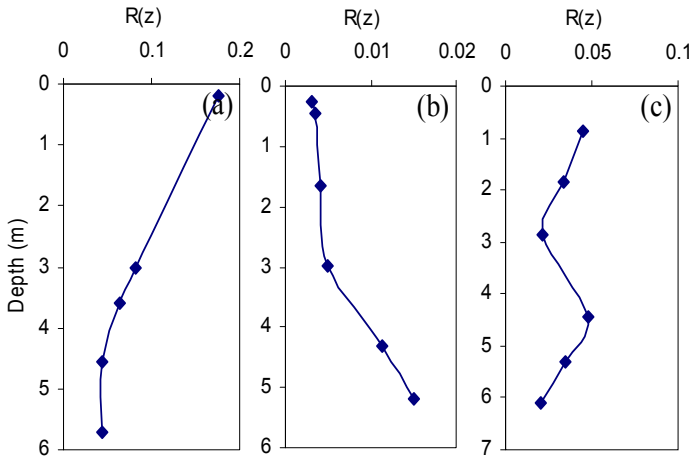

Fig. 10. Plots showing (a) decreasing, (b) increasing, (c) decreasing/increasing reflectance patterns for the wavelength 448nm.

Table 4. The variation of K_u and K_d for the decreasing subsurface reflectance [Fig. 10(a)]

Depth(m)	K_u	K_d	Case	Result
0.24	0.7358	0.7917	-	-
3.00	0.7199	0.4719	$K_u > K_d$	R decreases
3.58	0.9114	0.6319	$K_u > K_d$	R decreases
4.56	1.0183	0.7175	$K_u > K_d$	R decreases
5.72	0.9177	0.6750	$K_u > K_d$	R decreases

#206741 - $15.00 USD Received 19 Feb 2014; revised 14 Mar 2014; accepted 15 Mar 2014; published 14 Apr 2014

Table 5. The variation of K_u and K_d for the increasing subsurface reflectance [Fig. 10(b)]

Depth(m)	K_u	K_d	Case	Result
0.24	0.9345	1.4762	-	-
0.46	0.9679	1.5380	$K_u<K_d$	*R* increases
1.64	1.1040	1.3252	$K_u<K_d$	*R* increases
2.97	1.2356	1.3578	$K_u<K_d$	*R* increases
4.31	0.8298	1.1501	$K_u<K_d$	*R* increases
5.17	0.9439	1.2681	$K_u<K_d$	*R* increases

Table 6. The variation of K_u and K_d for the decreasing/increasing subsurface reflectance [Fig. 10(c)]

Depth(m)	K_u	K_d	Case	Result
0.87	0.9353	1.0064	-	-
1.83	1.3718	1.2111	$K_u>K_d$	*R* decreases
2.87	1.5592	1.3060	$K_u>K_d$	*R* decreases
4.43	1.7551	1.7716	$K_u<K_d$	*R* increases
5.28	2.0269	1.9351	$K_u>K_d$	*R* decreases
6.11	2.0269	1.7034	$K_u>K_d$	*R* decreases

7. Conclusion

In this paper, we have presented a novel model based on the large *in situ* data for computing subsurface irradiance reflectances in relatively clear, turbid and eutrophic waters. The key to such an improved model lies in the estimation of the *f* factor and its variation as a function of its dependent parameters throughout the water column. The model equation for *f* (just below the surface and subsurface) has been developed for different types of waters based on the solar angle, absorption coefficients and vertical attenuation coefficients of the upwelling and downwelling light fields. The results from the new model have shown excellent agreement with measurement data when compared to those of the existing models. These results further demonstrate that the parameter *f* is highly influenced by the absorption coefficients, solar zenith angle and downward and upward diffuse light fields in the water column. The new model is valid for homogeneous, inhomogeneous and stratified coastal/oceanic waters because of its improved parameterization based on the measurements from the various depths and water types. The advantage of the new model is that it does not require the bottom albedo for calculation of the reflectance at the ocean floor or at intermediate depths. Direct estimation of bottom albedo from field measurements is highly impossible due to its complexities and will introduce significant errors in the derived reflectance. Alternatively, consideration of the diffuse light fields, solar angle and IOPs in the model provides accurate (depth-wise) reflectances in the water column. Since the present model is dependent on the intermediate measurements, it may be considered as the drawback of the model. But generally for homogeneous waters, depth-wise measurements are absolutely not necessary, whereas for inhomogeneous/stratified waters the depth-wise measurements are necessary due to the variation of the IOPs. The effort made to study the influence of *f* on the reflectance provides satisfactory results (for just below the surface and throughout the water column) in a wide range of waters within the coastal and estuarine domains. Since the present model accounts for variations in *f*, many remote-sensing algorithms can be improved for coastal applications. The new model will have great significance for other applications including underwater imaging, diving and engineering operations.

Acknowledgments

This work was supported by grants from the NRB (Project Number OEC1112106NRBXPSHA). We would like to thank D. Rajasekhar, The Head, Vessel

Management Cell, and Director of National Institute of Ocean Technology (NIOT) for providing the Sagar Purvi (Coastal Research Vessel) to Indian Institute of Technology (IIT) Madras, Chennai, India for making the various bio-optical and underwater light field measurements. We are thankful to the anonymous reviewers for the constructive and valuable comments.

#206741 - $15.00 USD Received 19 Feb 2014; revised 14 Mar 2014; accepted 15 Mar 2014; published 14 Apr 2014